Thermodynamics around the first-order ferromagnetic phase transition of Fe_2P single crystals

M. Hudl,[1,2,*] D. Campanini,[3] L. Caron,[4] V. Höglin,[5] M. Sahlberg,[5] P. Nordblad,[6] and A. Rydh[3,†]

[1]*Department of Materials, ETH Zürich, Vladimir-Prelog-Weg 4, CH-8093 Zurich, Switzerland*

[2]*KTH Royal Institute of Technology, ICT Materials Physics, Electrum 229, SE-164 40 Kista, Sweden*

[3]*Department of Physics, Stockholm University, SE-106 91 Stockholm, Sweden*

[4]*Fundamental Aspects of Materials and Energy, Faculty of Applied Sciences, TU Delft Mekelweg 15, 2629 JB Delft, The Netherlands*

[5]*Department of Chemistry—Ångström, Uppsala University, Box 538, SE-751 21 Uppsala, Sweden*

[6]*Department of Engineering Sciences, Uppsala University, Box 534, SE-751 21 Uppsala, Sweden*

(Received 9 July 2014; revised manuscript received 8 October 2014; published 28 October 2014)

The specific heat and thermodynamics of Fe_2P single crystals around the first-order paramagnetic to ferromagnetic (FM) phase transition at $T_C \simeq 217$ K are empirically investigated. The magnitude and direction of the magnetic field relative to the crystal axes govern the derived H-T phase diagram. Strikingly different phase contours are obtained for fields applied parallel and perpendicular to the c axis of the crystal. In parallel fields, the FM state is stabilized, while in perpendicular fields the phase transition is split into two sections, with an intermediate FM phase where there is no spontaneous magnetization along the c axis. The zero-field transition displays a textbook example of a first-order transition with different phase stability limits on heating and cooling. The results have special significance since Fe_2P is the parent material to a family of compounds with outstanding magnetocaloric properties.

DOI: 10.1103/PhysRevB.90.144432 PACS number(s): 75.40.−s, 65.40.Ba, 65.40.G−, 75.30.−m

I. INTRODUCTION

First-order magnetic phase transitions (FOMTs) attract attention due to their promising applications in magnetic shape memory alloys [1,2], magnetic sensing based on colossal magnetoresistance [3], and magnetic refrigeration [4–8]. The FOMT may be driven by temperature, pressure, or applied magnetic field and is associated with a sudden change of structure or lattice parameters, resistivity, and magnetic entropy. Anisotropy and structural distortions play important roles for the FOMT. Materials with strong magnetic anisotropy, for instance, enable unusual and highly efficient ways in tuning magnetocaloric effects [9,10]. Di-iron phosphide, Fe_2P, is a hexagonal transition-metal pnictide with strong magneto-crystalline anisotropy that undergoes a first-order paramagnetic to ferromagnetic phase transition at ∼216 K [11–13]. The transition of Fe_2P is magnetoelastic, with a discontinuous isostructural change of the dimensions of the hexagonal unit cell [13] at the Curie temperature T_C. Below T_C the magnetic ordering occurs along the crystallographic c-axis direction [12]. The thermodynamics at the phase transition is of particular interest since Fe_2P is the parent compound for an entire class of tunable first-order magnetocaloric materials built on rare-earth-free constituents [14].

The anisotropic magnetic and magnetocaloric properties of Fe_2P were recently studied by Caron *et al.* [15]. Specific heat for polycrystalline Fe_2P in zero magnetic field has been studied earlier [16]. A deeper thermodynamic understanding of the FOMT is, however, lacking. In this work we report high-resolution nanocalorimetric specific-heat measurements of high-quality Fe_2P single crystals in applied magnetic fields both parallel and perpendicular to the c axis. We furthermore directly probe the latent heat of the FOMT. The results provide insights into the behavior of first-order systems with strong magnetic anisotropy and present a textbook example of diverging specific heat around first-order transitions in general.

II. EXPERIMENTAL DETAILS

High-quality single crystals of Fe_2P were grown in a tin melt [17,18]. Single-crystal x-ray-diffraction intensities in the ferromagnetic phase at 100 K were recorded on a Bruker diffractometer. The composition was refined to be $Fe_{1.995(2)}P$, where only the Fe(2) site is fully occupied. Magnetization measurements were performed using a Quantum Design magnetic property measurement system (MPMS XL SQUID) and physical property measurement system (PPMS 9-T VSM). Specific-heat measurements were performed using a differential membrane-based nanocalorimeter applying an ac method with phase stabilized frequency feedback [19]. The device allows measurements of μg size samples with both high resolution ($\Delta C/C \leqslant 10^{-4}$) and good absolute accuracy. Latent heat was measured with the same nanocalorimeter operating in a differential scanning mode. The single-crystal sample used for the specific-heat measurements was pillar shaped (length $189 \pm 9\,\mu$m) with a hexagonal basal plane (edges $31.9 \pm 4.3\,\mu$m).

III. EXPERIMENTAL RESULTS

The temperature dependence of the zero-field specific heat C_p is shown in Fig. 1(a). Specific-heat values obtained by Beckman *et al.* [16] at 150 K were used as a scale reference. The obtained sample mass agrees with the estimate from microscopy within uncertainties. The general temperature dependence and low-temperature behavior of the specific heat is in good agreement with the results in literature [16]. The specific heat associated with the FOMT appears as a sharp peak at the ferromagnetic-to-paramagnetic transition with $T_C \simeq 217$ K. The magnetic field dependence of the specific

*matthias.hudl@mat.ethz.ch, hudl@kth.se

†andreas.rydh@fysik.su.se

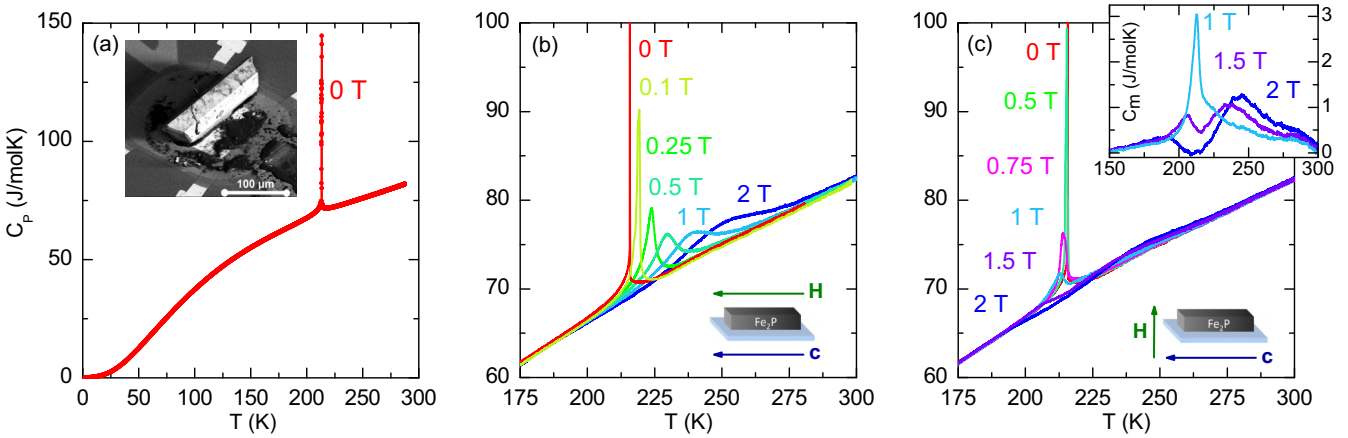

FIG. 1. (Color online) Temperature dependence of the specific heat of an Fe_2P crystal. (a) Specific heat in zero field. Inset: The sample mounted on the nanocalorimeter membrane cell. (b) Specific heat with magnetic field along the c axis (0, 0.1, 0.25, 0.5, 1, and 2 T). (c) Specific heat with field perpendicular to the c axis (0, 0.5, 0.75, 1, 1.5, and 2 T). Inset: The magnetic contribution C_m at high fields (1, 1.5, and 2 T).

heat in the vicinity of the phase transition is shown in Figs. 1(b) and 1(c). For fields $\mathbf{H} \parallel \mathbf{c}$, the transition is broadened and shifted to higher temperatures. When $\mathbf{H} \perp \mathbf{c}$, the location of the transition first appears nearly unchanged for fields below 0.5 T but is then split into two sections at higher fields [see Fig. 1(c)]. The lower transition shifts down in temperature while the upper one shifts to higher temperatures with increasing applied field, as is evident from the inset of Fig. 1(c), showing the magnetic contribution $C_m = C_{tot} - C_{bg}$ for high fields. The background specific heat C_{bg} is determined as an interpolation of the lowest specific heat for any field or field direction. There is quite a large torque at low temperatures for $\mathbf{H} \perp \mathbf{c}$. However, the very stiff Si_3N_4 calorimeter membrane does not allow any sample tilt but sustains the torque for small enough samples, as in the present case.

To investigate the character and latent heat of the FOMT, the specific heat in zero field was measured with a small temperature oscillation amplitude $T_{ac} < 160$ mK on very slow heating and cooling. As seen in Fig. 2(a), there is a clear hysteresis between heating and cooling, indicating a first-order transition [20,21]. By using the ac method with a small temperature oscillation amplitude on a small single crystal, the true specific heat is measured, without admixture of latent heat in the signal. At the supercooling and superheating stability limits T_0 and T_1 the system undergoes an instantaneous transition between the involved states. To quantify the latent heat of the transition, the calorimeter was turned into differential scanning mode, where the temperature difference between sample and reference calorimetric cells was measured at high speed during a slow base temperature scan. The latent heat at the transition gives rise to a sudden adiabatic temperature change ΔT of the sample and a subsequent temperature relaxation, as shown in Fig. 2(b). We find that the temperature increases by $\Delta T = 372$ mK when going from high to low temperature in zero applied field, corresponding to a latent heat of $L = 26.4$ J/mol or an entropy change $\Delta S_L = L/T_C = 122$ mJ/mol K ≈ 0.015 R. In magnetic fields $\mathbf{H} \perp \mathbf{c}$ the latent heat first decreases and finally vanishes for H slightly higher than 0.5 T. At 0.5 T, the latent heat is about 15% of that in zero field. Magnetic fields $\mathbf{H} \parallel \mathbf{c}$, on the other hand, quickly suppress the first-order character already below 0.1 T. As seen in Fig. 2(a), there is a divergent behavior of the zero-field specific heat on approaching the FOMT. However, this divergence does not occur around the equilibrium temperature T_C, but at the stability limits T_0 and T_1. This is expected for a first-order transition [20]. The temperature dependence of C_m is well described by a power law of the type $C_m = (\Gamma_\pm/n) \cdot |\varepsilon|^{-n}$ [22,23], where $\varepsilon = 1 - T/T_i$; n is an exponent; $i = 0, 1$; and $\Gamma_\pm$ are fitting parameters for $\varepsilon > 0\,(+)$ using $T_0 = 216.64$ K and $\varepsilon < 0$ $(-)$ using $T_1 = 217.52$ K, respectively. From fitting, using data in the reduced temperature range $5\times10^{-4} < \varepsilon < 10^{-2}$, we find $n = -0.006 \pm 0.01$ and a ratio $\Gamma_+/\Gamma_- = 1.006 \pm 0.01$ (not to be confused with the critical values of second-order phase transitions).

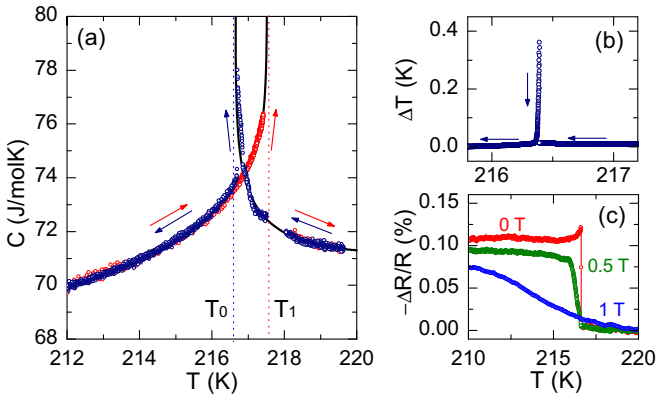

FIG. 2. (Color online) (a) Specific heat of an Fe_2P single crystal around the zero-field transition. The paramagnetic state supercools to a temperature T_0 while the ferromagnetic state superheats to T_1. The specific heat diverges at these corresponding temperatures rather than at T_C, following $C = C_0 + C_1T + C_m$ as shown by the solid curves. (b) Differential temperature $\Delta T = T_{sample} - T_{ref}$ as a function of reference temperature on cooling in zero field. A sudden temperature change of the sample is seen when the latent heat is released during the transition. (c) Persistent thermometer resistance change of the calorimeter due to the thermal expansion at the magnetoelastic transition of the sample for fields $\mathbf{H} \perp \mathbf{c}$.

When decreasing the temperature across the transition in zero magnetic field, the c axis undergoes a sudden contraction by 0.084% while the in-plane lattice parameter expands by 0.074% [12]. These thermal expansions can be sensed by the thin-film thermometer of the calorimeter, acting as a thermal expansion gauge. While this method does not give absolute values of volume changes, it provides a good account for the location and character of the isostructural transition. Figure 2(c) shows the signal from thermal expansion during cooling in magnetic fields $\mathbf{H} \perp \mathbf{c}$. As seen in the figure, the magnitude of the structural transition is suppressed by the magnetic field, and the transition is broadened and shifted toward lower temperatures. The structural change in a field of 0.5 T still amounts to more than 60% of that in zero field, while the latent heat has been significantly decreased. From this, we conclude that the latent heat associated with the structural transition itself is at most a minor part ($\lesssim$10%) of the total latent heat.

To understand the nature of the observed transitions, the specific-heat measurements were complemented with magnetization measurements. The field dependence of the magnetization is shown in Fig. 3(a) for $\mathbf{H} \parallel \mathbf{c}$ (solid curves) and $\mathbf{H} \perp \mathbf{c}$ (dashed curves), and the corresponding temperature dependence is shown in Fig. 3(b). Since the demagnetization effects are complicated by the strong anisotropy, applied fields rather than internal fields are used. The results agree well with Ref. [15]. As seen from Fig. 3, the system orders spontaneously along the c axis below the Curie temperature $T_C = 217$ K. The sharp increase of magnetization at T_C is accompanied by thermal hysteresis ($\lesssim$1 K), indicating first-order character of the phase transition. With increasing fields along the c axis, the transition temperature to the ferromagnetic state is quickly shifting to higher temperatures. However, for $\mathbf{H} \perp \mathbf{c}$ the magnetization suddenly starts to decrease below T_C, creating a cusp-shaped magnetization curve.

IV. DISCUSSION

Comparable magnetic behaviors are seen, e.g., for the paramagnetic-to-ferromagnetic transitions in MnP [9] and $DyAl_2$ [24–26]. This behavior can be understood by considering the magnetocrystalline anisotropy. At low fields along the c axis, the system orders spontaneously at T_C. A perpendicular applied field ($\mathbf{H} \perp \mathbf{c}$) tilts the magnetization vector away from the c axis. When the field reaches the anisotropy field, the c-axis component goes to zero. At constant field the magnetization $\mathbf{M}_{\perp \mathbf{c}}$ is suppressed below a certain temperature (and exhibits a cusp) due to an increasing magnetocrystalline anisotropy with decreasing temperature and the onset of magnetic ordering along the c axis.

The effects of the applied magnetic fields are well illustrated through the magnetic entropy. The magnetic entropy S_m can be obtained from the specific-heat measurements of Fig. 1 as the integral of C_m/T over temperature. Putting $S_m(300\,\mathrm{K}) = 0$ as a reference point, the thus obtained curves for $H = 0$ and 1 T applied along and perpendicular to the c axis are shown in Fig. 4(a). In zero field (black curve), the entropy increase ΔS_L due to the latent heat is added as a step function at T_C. It is seen that the magnetic entropy for $\mathbf{H} \parallel \mathbf{c}$ (blue curve) is lower than that of zero field, both above and below T_C. For $\mathbf{H} \perp \mathbf{c}$ (hard axis) the entropy is higher than for $\mathbf{H} \parallel \mathbf{c}$ at all temperatures.

Interestingly, $S_m(1\,\mathrm{T})$ is crossing $S_m(0\,\mathrm{T})$ at T_C, making the low-temperature entropy for $\mathbf{H} \perp \mathbf{c}$ higher than that of zero field [Fig. 4(a)]. This effect is clearly seen in Fig. 4(b), showing the magnetic entropy change $\Delta S_m = S_m(1\,\mathrm{T}) - S_m(0\,\mathrm{T})$. The magnetic entropy change ΔS_m due to a magnetization process can be calculated from magnetization data (Fig. 3) using Maxwell relations $[\Delta S_m(T,H) = \mu_0 \int_0^H (dM(T,H)/dT)dH]$ [4]. The thus derived ΔS_m are shown as open symbols in Fig. 4(b). The general behaviors of ΔS_m obtained from specific heat and magnetization are in good agreement, with the results from magnetic measurements giving a value ~10% higher at the position of the zero-field transition. The observed discontinuous change of the entropy at the FOMT indicates that the numerical evaluation is done without accumulated numerical errors [27].

For $\mathbf{H} \parallel \mathbf{c}$, a strong magnetocaloric effect (entropy is decreasing with increasing field) is seen as a dip in ΔS_m.

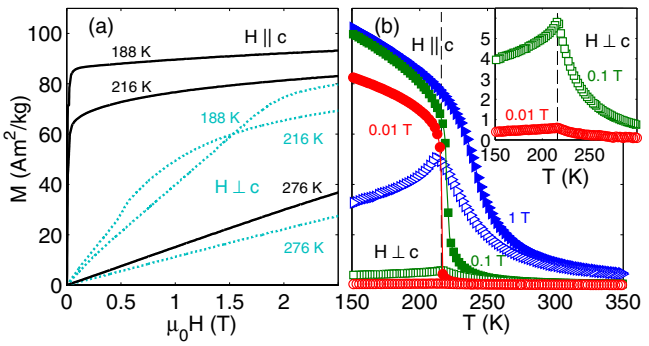

FIG. 3. (Color online) Magnetization along the applied field of an Fe_2P crystal. (a) Magnetization as a function of field applied along the c axis (solid curves) and perpendicular to the c axis (dashed curves) for three different temperatures: 188 K, 216 K $\approx T_C$, and 276 K. (b) Temperature dependence of the magnetization for fields along (filled symbols) and perpendicular to (open symbols) the c axis ($\circ = 0.01$ T, $\square = 0.1$ T, and $\triangleright = 1$ T). Inset: The low-field curves for $\mathbf{H} \perp \mathbf{c}$. $T_C(0\,\mathrm{T})$ is indicated by vertical dashed lines.

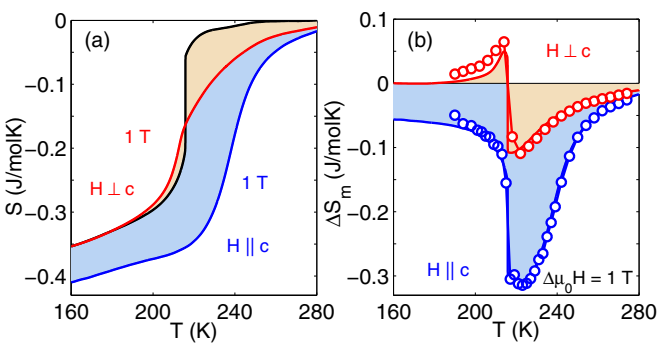

FIG. 4. (Color online) (a) Magnetic entropy S_m around T_C calculated from specific-heat data in 0 T (black curve) and 1 T with field applied along (blue curve) and perpendicular to the c axis (red curve). (b) The magnetic entropy change $\Delta S_m = S_m(H) - S_m(0)$ obtained from specific heat (solid curves) and magnetic measurements (symbols), with field applied along (blue) and perpendicular to the c axis (red).

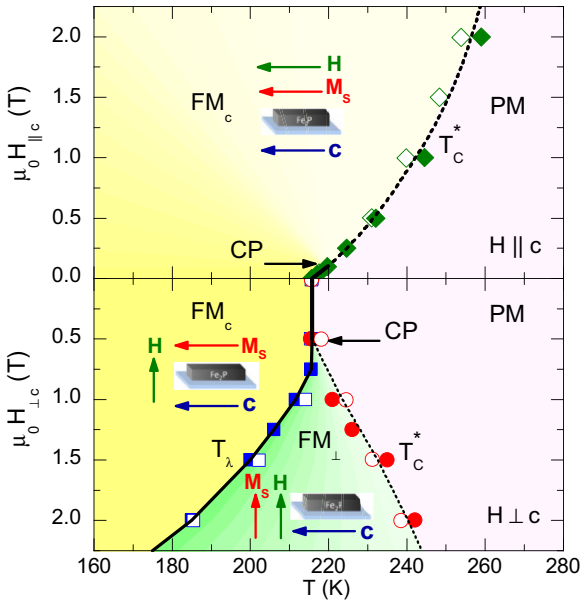

FIG. 5. (Color online) Magnetic phase diagram for Fe_2P obtained from specific heat (filled symbols) and magnetization measurements (open symbols), complemented with published results [15]. The upper panel shows the phase diagram for magnetic field applied along the c axis, while the lower panel shows the case for $\mathbf{H} \perp \mathbf{c}$ (with reversed ordinate). The direction of M_s is indicated for each ferromagnetic phase. The transition is first order for fields below the directional-dependent critical point, marked CP.

However, for $\mathbf{H} \perp \mathbf{c}$, a positive ΔS_m is found below T_C, corresponding to an *inverse* magnetocaloric effect. This positive magnetic entropy change reflects an increased disorder of the spin system in the temperature range where the applied magnetic field and the effective magnetocrystalline anisotropy are of equal strength (near the cusps in M versus T). Increased disorder of the spin system should be reflected in a decreased total magnetization with increasing field in this area. This is indeed seen from measurements of the total magnetization [15].

The derived H-T magnetic phase diagram for Fe_2P is shown in Fig. 5. At low fields $\mathbf{H} \parallel \mathbf{c}$ (upper panel), T_C is shifted to higher temperatures, forming a line of first-order phase transitions that ends at a critical point $\mu_0 H_{\parallel,cr} < 0.1$ T. Above the critical point, the continuation of the phase transition is determined from the maximum in specific heat at different applied fields (filled symbols in Fig. 5) and the maximum of dM/dT at constant field (open symbols), agreeing well with each other. For the case of $\mathbf{H} \perp \mathbf{c}$, the lower panel of Fig. 5, the first-order transition extends up to a critical or possibly tricritical point $\mu_0 H_{\perp,cr} \approx 0.5$ T. For fields above $H_{\perp,cr}$ two characteristic temperatures are observed in the magnetization and specific heat, indicated by $T_C^\star$ (increasing with increasing magnetic field) and T_λ (decreasing with increasing field) in Fig. 5. The minimum in dM/dT closely coincides with $T_C^\star$ as obtained from specific heat. The lower characteristic temperature corresponding to T_λ is taken as the maximum in dM/dT below the peak in magnetization (see Fig. 3), which decreases with increasing field and roughly coincides with the T_λ found from specific heat, as seen in the lower panel of Fig. 5.

The magnetic entropy change ΔS_L at the first-order part of the transition line $T_C^\star(H)$ is related to the jump in magnetization ΔM and slope of the phase boundary through the magnetic analog of the Clausius-Clapeyron equation: $dT_C^\star/d(\mu_0 H) = -\Delta M/\Delta S_L$. With ΔM from Fig. 3 and ΔS_L from the latent heat measurements, we calculate the initial slope of the phase transition line to be 59 K/T. From the data shown in Fig. 5 we find $dT_C^\star/d(\mu_0 H) = 38$ K/T for fields $\leqslant 0.1$ T along the c axis. For $\mathbf{H} \perp \mathbf{c}$, on the other hand, there is no magnetization jump along the applied field at $T_C^\star$. Thus, $T_C^\star$ is independent of H for this field direction, up to the critical point $\mu_0 H_{\perp,cr}$ where ΔS_L goes to zero.

To interpret the full phase diagram, first note that the zero-field transition is a combined elastic and magnetic transition from a paramagnetic (PM) phase into a ferromagnetic phase ordered along the c axis (FM_c). For $\mathbf{H} \parallel \mathbf{c}$ (Fig. 5), it is clear that magnetic fields applied in this direction stabilize the FM_c phase. For $\mathbf{H} \perp \mathbf{c}$ at low fields ($H < H_{\perp,cr}$), the location of the PM-to-FM_c phase boundary is unaffected by the applied field, similarly indicating that its spontaneous magnetization direction is perpendicular to the field in this case. However, at higher fields a new phase appears between T_λ and $T_C^\star$, indicated as $FM_\perp$. This phase represents a state *without* spontaneous magnetization M_s along the c axis, but with ferromagnetic order stabilized by the applied field. At the transition line T_λ the nature of the anisotropy changes from a pure uniaxial character with linear increase of the magnetization with increasing perpendicular fields into a regime with higher-order anisotropy terms. This can be seen from the M versus H curves in Fig. 3(a), where an increase of the field causes further alignment of the magnetization along the applied field. Such a behavior is different from the reordering transition discussed in literature [9,28], where the spin reordering has a first-order nature. The elastic transition is closely following the onset of magnetic ordering along the c axis, i.e., along $T_C^\star$ for $\mathbf{H} \parallel \mathbf{c}$ and T_λ for $\mathbf{H} \perp \mathbf{c}$. Since the elastic transition does not bring much latent heat, it is likely that it is driven by the FM_c ordering.

V. CONCLUSION

In conclusion, we have found that the low-field FOMT of Fe_2P ends at a critical point governed by strong magnetocrystalline anisotropy. For fields applied perpendicular to the c axis, the low-temperature ferromagnetic state displays increasing magnetic entropy with increasing field, corresponding to a negative magnetocaloric effect. At higher temperatures and fields a new phase $FM_\perp$ appears, where the c-axis anisotropy becomes ineffective. This implies an orientational order (along the c axis) to disorder transition with increasing temperature at the T_λ phase line. The structural (elastic) transition is found to be linked to this c-axis ordering and exhibits associated latent heat at low fields of $\lesssim$10% of the total latent heat.

ACKNOWLEDGMENTS

Financial support from the Swedish Research Council - Vetenskapsrådet (Contract No. 2012-6562) is acknowledged. We thank M. Fiebig (ETH) and O. Tjernberg (KTH) for hosting M.H. during his postdoctoral studies and E. Brück, Z. Diao, and V. M. Krasnov for useful discussions.

[1] V. Chernenko and S. Besseghini, Sensors and Actuators A (Physical) **142**, 542 (2008).

[2] J. Enkovaara, A. Ayuela, A. T. Zayak, P. Entel, L. Nordström, M. Dube, J. Jalkanen, J. Impola, and R. Nieminen, Mater. Sci. Eng. A **378**, 52 (2004).

[3] A. P. Ramirez, J. Phys.: Condens. Matter **9**, 8171 (1997).

[4] A. M. Tishin and Y. I. Spichkin, in *The Magnetocaloric Effect and its Applications*, edited by J. M. D. Coey, D. R. Tilley, and D. R. Vij (IOP Publishing, Bristol, Philadelphia, 2003).

[5] K. A. Gschneidner, Jr., V. K. Pecharsky, and V. K. Tsokol, Rep. Prog. Phys. **68**, 1479 (2005).

[6] B. Shen, J. Sun, F. X. Hu, H. Zhang, and Z. Cheng, Adv. Mater. **21**, 4545 (2009).

[7] N. de Oliveira and P. von Ranke, Phys. Rep. **489**, 89 (2010).

[8] G. F. Wang, Ph.D. thesis, Universidad de Zaragoza, 2012.

[9] M. S. Reis, R. M. Rubinger, N. A. Sobolev, M. A. Valente, K. Yamada, K. Sato, Y. Todate, A. Bouravleuv, P. J. von Ranke, and S. Gama, Phys. Rev. B **77**, 104439 (2008).

[10] S. A. Nikitin, K. P. Skokov, Y. S. Koshkid'ko, Y. G. Pastushenkov, and T. I. Ivanova, Phys. Rev. Lett. **105**, 137205 (2010).

[11] R. Wäppling, L. Häggström, T. Ericsson, S. Devanarayanan, E. Karlsson, B. Carlson, and S. Rundqvist, J. Solid State Chem. **13**, 258 (1975).

[12] H. Fujii, T. Hokabe, T. Kamigaichi, and T. Okamoto, J. Phys. Soc. Jpn. **43**, 41 (1977).

[13] L. Lundgren, G. Tarmohamed, O. Beckman, B. Carlsson, and S. Rundqvist, Phys. Scr. **17**, 39 (1978).

[14] N. H. Dung, Z. Q. Ou, L. Caron, L. Zhang, D. T. Cam Thanh, G. A. de Wijs, R. A. de Groot, K. H. J. Buschow, and E. Brück, Adv. Energy Mater. **1**, 1215 (2011).

[15] L. Caron, M. Hudl, V. Höglin, N. H. Dung, C. P. Gomez, M. Sahlberg, E. Brück, Y. Andersson, and P. Nordblad, Phys. Rev. B **88**, 094440 (2013).

[16] O. Beckman, L. Lundgren, P. Nordblad, P. Svedlind, and A. Törne, Phys. Scr. **25**, 679 (1982).

[17] R. Madar, P. Senateur, and R. Fruchart, in *Proceedings of the Fifth International Conference on Crystal Growth, 1977* (unpublished).

[18] Y. Anderson, S. Rundqvist, O. Beckman, L. Lundgren, and P. Nordblad, Phys. Stat. Sol. A **49**, K153 (1978).

[19] S. Tagliati, V. M. Krasnov, and A. Rydh, Rev. Sci. Instrum. **83**, 055107 (2012).

[20] K. Binder, Rep. Prog. Phys. **50**, 783 (1987).

[21] S. B. Roy, J. Phys.: Condens. Matter **25**, 183201 (2013).

[22] D. Kim, B. L. Zink, F. Hellman, and J. M. D. Coey, Phys. Rev. B **65**, 214424 (2002).

[23] A. Kornblit and G. Ahlers, Phys. Rev. B **8**, 5163 (1973).

[24] P. J. von Ranke, I. G. de Oliveira, A. P. Guimarães, and X. A. da Silva, Phys. Rev. B **61**, 447 (2000).

[25] A. L. Lima, A. O. Tsokol, K. A. Gschneidner, V. K. Pecharsky, T. A. Lograsso, and D. L. Schlagel, Phys. Rev. B **72**, 024403 (2005).

[26] P. J. von Ranke, N. A. de Oliveira, D. C. Garcia, V. S. R. de Sousa, V. A. de Souza, A. M. G. Carvalho, S. Gama, and M. S. Reis, Phys. Rev. B **75**, 184420 (2007).

[27] M. Kataoka, T. Kanomata, R. Y. Umetsu, and R. Kainuma, J. Magn. Magn. Mater. **361**, 34 (2014).

[28] C. C. Becerra, V. Bindilatti, and N. F. Oliveira, Jr., Phys. Rev. B **62**, 8965 (2000).